



Contents lists available at ScienceDirect

Remote Sensing of Environment

journal homepage: www.elsevier.com/locate/rse

Monitoring elevation variations in leaf phenology of deciduous broadleaf forests from SPOT/VEGETATION time-series

Dominique Guyon^{a,*}, Marie Guillot^a, Yann Vitasse^{b,c}, Hervé Cardot^d, Olivier Hagolle^e, Sylvain Delzon^{b,c}, Jean-Pierre Wigneron^a

^a INRA, UR1263 EPHYSE, F-33140 Villenave d'Ornon, France

^b INRA, UMR BIOGECO, F-33610 Cestas, France

^c Université de Bordeaux, UMR BIOGECO, Av. des Facultés, F-33405 Talence, France

^d Université de Bourgogne, CNRS, UMR 5584, Institut de Mathématiques de Bourgogne, BP 47870, F-21078 Dijon, France

^e CESBIO, Unité mixte CNES CNRS IRD UPS, 18 avenue E. Belin, F-31401 Toulouse Cedex 9, France

ARTICLE INFO

Article history:

Received 9 January 2010

Received in revised form 12 October 2010

Accepted 16 October 2010

Available online xxxx

Keywords:

Phenology

Leaf unfolding

Deciduous forest

Elevation

VEGETATION

Perpendicular vegetation index

Temporal unmixing

ABSTRACT

In mountain forest ecosystems where elevation gradients are prominent, temperature gradient-based phenological variability can be high. However, there are few studies that assess the capability of remote sensing observations to monitor ecosystem phenology along elevation gradients, despite their relevance under climate change. We investigated the potential of medium resolution remotely sensed data to monitor the elevation variations in the seasonal dynamics of a temperate deciduous broadleaf forested ecosystem. Further, we explored the impact of elevation on the onset of spring leafing. This study was based on the analysis of multi-annual time-series of VEGETATION data acquired over the French Pyrenees Mountain Region (FPMR), in conjunction with simultaneous ground-based observations of leaf phenology made for two dominant tree species in the region (oak and beech). The seasonal variations in the perpendicular vegetation index (PVI) were analyzed during a five-year period (2002 to 2006). The five years of data were averaged into a one sole year in order to fill the numerous large spatio-temporal gaps due to cloud and snow presence – frequent in mountains – without altering the temporal resolution. Since a VEGETATION pixel (1 km²) includes several types of land cover, the broadleaf forest-specific seasonal dynamics of PVI was reconstructed pixel-by-pixel using a temporal unmixing method based on a non-parametric statistical approach. The spatial pattern of the seasonal response of PVI was clearly consistent with the relief. Nevertheless the elevational or geographic range of tree species, which differ in their phenology sensitivity to temperature, also has a significant impact on this pattern. The reduction in the growing season length with elevation was clearly observable from the delay in the increase of PVI in spring and from the advance of its decrease in the fall. The elevation variations in leaf flushing timing were estimated from the temporal change in PVI in spring over the study area. They were found to be consistent with those measured *in situ* ($R^2 > 0.95$). It was deduced that, over FPMR, the mean delay of leaf flushing timing for every 100 m increase in elevation was estimated to be approximately 2.3 days. The expected estimation error of satellite-based leaf unfolding date for a given elevation was approximately 2 days. This accuracy can be considered as satisfactory since it would allow us to detect changes in leafing timing of deciduous broadleaf forests with a magnitude equivalent to that due to an elevation variation of 100 m (2.3 days on average), or in other words, to that caused by a variation in the mean annual air temperature of 0.5 °C. Although averaging the VEGETATION data over five years led to a loss of interannual information, it was found to be a robust approach to characterise the elevation variations in spring leafing and its long-term trends.

© 2010 Elsevier Inc. All rights reserved.

1. Introduction

Vegetation phenology namely the timing of the plant activity as influenced by the environment seasonality is a relevant indicator of

the response of terrestrial ecosystems to global warming (Cleland et al., 2007). Many studies have documented the phenological changes observed across the northern hemisphere in recent decades (see the review paper of Cleland et al., 2007). Earlier spring events (leafing, flowering) and longer growing seasons are some of the most significant changes in the vegetation seasonal cycle in the boreal and temperate zones. Analyses of long-term *in situ* observations have demonstrated the clear advancement of the start of spring at species

* Corresponding author. INRA, UR1263 EPHYSE, BP81, F-33884 Villenave d'Ornon Cedex, France. Tel.: +33 5 57 12 24 29; fax: +33 5 57 12 24 20.

E-mail address: guyon@bordeaux.inra.fr (D. Guyon).

level (e.g. for Europe: Menzel & Fabian, 1999; Menzel et al., 2006). Satellite-based observations have revealed the shifts in leaf phenology of ecosystems at global scale (Myneni et al., 1997; Zhou et al., 2001).

Retrospective approaches are crucial to quantify the phenological shifts and to link them to climate change. Remote sensing time-series data offering an extensive coverage of land surfaces complement the long-term records provided by ground observation networks and historical reconstructions (Rutishauser et al., 2007), although their temporal coverage spans only the most recent 30 years.

The use of daily data at medium spatial resolution provided by satellite sensors such as AVHRR, MODIS or VEGETATION to investigate the timing of vegetation green-up (Beck et al., 2006; Delbart et al., 2006; Fisher et al., 2006; Maignan et al., 2008; Soudani et al., 2008; Zhang et al., 2003), and its interannual changes or its long-term trends (Delbart et al., 2006; Maignan et al., 2008; Myneni et al., 1997; Stöckli & Vidale, 2004; Zhou et al., 2001) on large extents has been widely developed during the last decade. These numerous studies benefited from substantial improvements in the reconstruction of land surface reflectance time-series, in particular due to the recent advances in filtering of cloudy or snowy pixels, correction of atmospheric disturbances and normalisation of directional effects (Bacour et al., 2006; Hagolle et al., 2005) and also to the launch of new sensors of higher quality (Badeck et al., 2004) in geometry and radiometry. The timing of phenology of forest ecosystems from remote sensing is commonly based on the analysis of the seasonal trajectory of vegetation indices (e.g. NDVI) pixel-by-pixel. The onset and the end of the growing season are identified from the increase of vegetation index in spring and its decrease in autumn with time. For this purpose the seasonal variations in vegetation index are modelled. Several approaches are possible. Non-parametric methods with various temporal or spatio-temporal interpolation algorithms have been developed (Beck et al., 2006; Maignan et al., 2008; Stöckli & Vidale, 2004). Statistical fitting of predefined curves (e.g. double logistic function) has also been used with the assumption that the vegetation dynamics is known *a priori*, ignoring the effects of disturbance (Fisher et al., 2006; Zhang et al., 2003). The timing of phenological transitions is then inferred either by thresholding the modelled vegetation index at a predefined value (Delbart et al., 2006; Maignan et al., 2008) or by using some parameters of the fitted parametric functions (Beck et al., 2006; Fisher et al., 2006; Soudani et al., 2008; Zhang et al., 2003) such as the inflection points.

The coarse spatial resolution of the most commonly used datasets – 8 km for AVHRR or 1 km for MODIS and VEGETATION – is relevant to relate the phenology global patterns to climate warming, as shown by the studies applied to global or continental scales on large latitude ranges (Delbart et al., 2006; Maignan et al., 2008; Myneni et al., 1997; Stöckli & Vidale, 2004; Zhou et al., 2001). However, as a given pixel contains a mixture of different species and land-cover types, it is not easy to clearly extract the phenological response of a given type of vegetation (Badeck et al., 2004). Also, Fisher et al. (2007) highlighted that, in deciduous forests, the mixture of species differing in their phenological behaviour makes it difficult to understand the link between satellite information and temperature variability if the species composition is unknown. The temporal unmixing is then a useful approach to downscale from the medium resolution pixel to the local seasonal dynamics of each land-use or vegetation type (Cardot et al., 2008).

Mountain forest ecosystems where the phenology variability can be observed along the broad temperature gradient associated with the large elevation gradient are particularly vulnerable to global warming. Consequences can already be observed on the elevation range of species (Bertin, 2008; Lenoir et al., 2008; Peñuelas & Boada, 2003). Species can either adapt via their phenotype plasticity and/or their genetic diversity, phenological changes reflecting the adaptive response of species, or migrate to milder elevations. However distributional changes are likely to be much slower than the phenological changes (Bertin, 2008). Moreover the climate forcing does not completely explain the observed

elevation shifts in plant species as there are some other confounding factors such as changes in land management (Peñuelas & Boada, 2003).

A few studies (e.g. Vitasse et al., 2009a,b) have investigated the seasonal forest species dynamics along elevation gradients and papers based on remote sensing are rare. Beck et al. (2008) presented the gradation of the seasonal course of NDVI derived from MODIS time-series depending on elevation in a mountainous area of China; with a clear decrease in the duration of the green-up period over a 1500 m gradient. Using high resolution data (Landsat TM at 30 m), Fisher et al. (2006) have quantified the effect of the local topography on the initiation of growing season. The too coarse resolution of global 8-km AVHRR data did not allow Maignan et al. (2008) to capture the effect of temperature variations on the onset of the growing season of mountain forests in Switzerland because of the high within-pixel heterogeneity in elevation and vegetation.

In this paper, we investigated the potential of medium resolution remote sensing to monitor the elevation variations in the seasonal dynamics of temperate deciduous broadleaf forests and to estimate the impact of the elevation on the spring leafing timing of deciduous species. This study is based on a multi-annual time-series of VEGETATION data (2002 to 2006) acquired over an area with large elevation gradients in the French Pyrenees mountains region. Although the spatial resolution (1-km) of this dataset is coarser than that of some MODIS land products (250 and 500 m), we chose to use the VEGETATION observations for the following reasons. Firstly, VEGETATION observations were corrected for the directional effects, which was not the case for the MODIS reflectance products available at the finest resolution (250 m). Secondly, the temporal frequency of the reconstructed reflectance time-series is larger (three times a month) than the one given by the MODIS nadir adjusted reflectance products available at 500 m resolution (two times a month). An unmixing technique was then applied to retrieve the pure seasonal course of reflectance signal of the broadleaf forests pixel-by-pixel. The analysis of the satellite time-series to retrieve the timing of leaf unfolding was supported by the availability of simultaneous *in situ* observations of phenology for the two main deciduous species in the study area – oak and beech.

2. Materials and methods

2.1. Study area

The study was carried out in a 135 km × 100 km area which covers a large part of the Pyrenean region in South-West France between longitudes 1.24°W to 0.25°E and latitudes 42.71°N to 43.61°N (Fig. 1). This area is characterized by a temperate oceanic climate, with a mean annual temperature of 12 °C and a mean annual precipitation of 1079 mm (observations of Météo-France from 1946 to 2001 in Tarbes, 43°11'N, 00°00'W, 360 m asl (above sea level)). The elevation varies from 0 m asl in the plains in the North, to 3100 m in the Pyrenees Mountains in the South. The upper elevation limit of broadleaf forests is approximately 1800 m, whereas the tree line of coniferous and mixed forests is approximately 2000 m. Oak (mainly sessile oak, *Quercus petraea*) and beech (*Fagus sylvatica*) are the main deciduous broadleaf species of the study area. Their distribution differs according to elevation; oak occurs over elevations lower than beech as shown in Fig. 2, even though it is still present at high elevation.

Geographical information on the elevation and the land use were respectively derived from the Shuttle Radar Topography Mission (USGS, 2005) and the European CLC2000 database (EEA, 2000).

2.2. Field phenological observations

We used the phenological data set measured by Vitasse et al. (2009b) over the study area. The leaf unfolding of sessile oak and beech was monitored at ground level over 22 sites during three

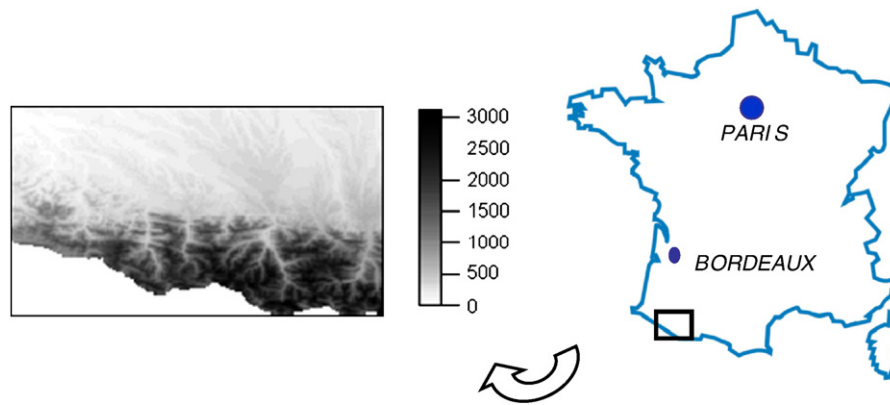


Fig. 1. Location and elevation (asl, in meters) of the study area. White: mask over Spain.

consecutive years from 2005 to 2007. The sites were located in hilly and mountain areas along two transects following two valleys: the Ossau valley (Pyrénées Atlantiques) and the Gave valley (Hautes Pyrénées). These were more or less parallel and at a distance of approximately 30- to 50-km apart. Elevation increases from North to South along each transect and the temperature lapse rate over the elevation gradient was approximately $0.4\text{ }^{\circ}\text{C}$ for every 100 m increase in elevation (Vitasse et al., 2009a,b).

Both species were sampled in each transect at five elevation levels: 100 m, 400 m, 800 m, 1200 m and 1600 m above sea level (± 50 m). Four intermediate levels were added in the Gave valley for oak: 350 m, 600 m, 1000 m, and 1300 m. In this way 10 populations of beech and 14 populations of sessile oak were selected. The timing of leaf unfolding (LU) was monitored *in situ* every ten days over ten dominant and mature trees sampled in each population. The exact date of LU (LUD) of each tree sample was estimated by linear interpolation between the measurement dates. At the population level, LUD was calculated as the mean of the ten individual values. Details on the spatial sampling of elevation and on the method used for the phenological observations are given by Vitasse et al. (2009a,b).

Measurements of the elevation variations in LUD from 2005 to 2007 for oak and beech populations are given in Fig. 3a (Vitasse et al., 2009a,b). Both species showed different elevation patterns of LUD and LUD appears to be more sensitive to the elevation gradient for oak than for beech (3.2 and 1 days. 100 m^{-1} , respectively). To simulate the expected mean variations in deciduous forests LUD (LUDd) depending on the elevation for the mean climatic conditions over the three years, we combined the phenological patterns of the two species (equations given in Fig. 3a) with a weighting corresponding to their relative elevation distribution (given in Fig. 2). LUDd elevation variations were found to be similar to the LUD elevation variations of beech at an elevation greater than 900 m. At lower elevations LUDd was delayed by 5 to 6 days in comparison with the LUD of pure oak

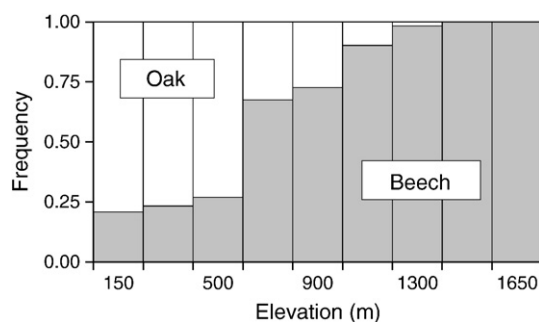


Fig. 2. Elevation repartition of the deciduous broadleaf species: presence frequency of oak versus beech, according to statistics provided by the French office of national forest inventory (Inventaire Forestier National, IFN) from $n = 1052$ ground observations. Frequency of oak = $1 -$ frequency of beech.

stands (Fig. 3b), even though its sensitivity to elevation gradient was similar (the slope of LUD as function of elevation is approximately 3 days. 100 m^{-1} in both cases). The mean delay of LUDd due to a 100 m elevation increase was approximately 2.3 days over the whole elevation range. In this study, we will consider the curve of LUDd (Fig. 3b) corresponds to the elevation pattern of LUD variations of broadleaf forests by assuming that the latter were composed of only oak and beech. With the same assumption, the mean LUD of broadleaf forests (denoted as LUD_{REF}) in 2005, 2006 and 2007 was approximated by averaging LUDd as a function of elevation over the study area, with a weighting by the elevation distribution of surface fraction containing broadleaf forests derived from CLC2000 database. LUD_{REF} was equal to 105.5 (15 April).

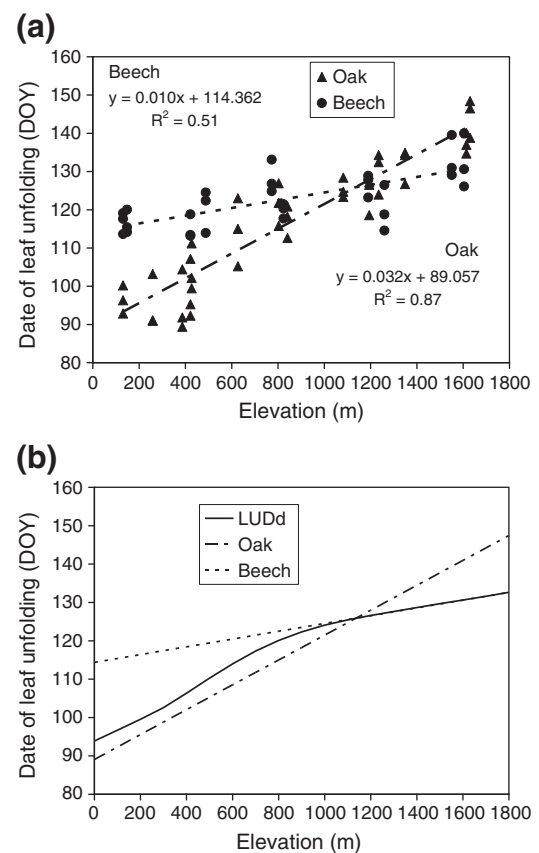


Fig. 3. Dates of the leaf unfolding of deciduous species observed at ground level in 2005, 2006 and 2007 as a function of elevation: (a) Observations for beech (*Fagus sylvatica*) and oak (*Quercus petraea*) (Vitasse et al., 2009b), (b) Elevation patterns of the two species and their weighted average (LUDd). DOY is day of the year.

2.3. VEGETATION data

A multi-annual time-series of reflectance data was produced at sampling intervals of 10 days for five years from 2002 to 2006, by using daily data from VEGETATION 1 and VEGETATION 2 instruments on board SPOT-4 and SPOT-5 satellites. After the correction of the sensors sensitivity drift and atmospheric effects, the compositing per 10-day period was performed including the elimination of cloudy or snowy observations and the normalisation of directional effects. The latter was performed with Roujean's model (Roujean et al., 1992), which was fitted to non-cloudy and non-snowy observations gathered over a time window of ± 15 days from the middle of the compositing interval. The core algorithm used is given in Hagolle et al. (2005) and Baret et al. (2007). Finally, the 10-day data produced was the top of canopy reflectance in each spectral band (red, near infrared and shortwave infrared) normalised at view zenith angle = 0° and at sun zenith angle at 10:30 UT for the median day of the ten-day compositing period. It was delivered under the lat–lon projection at $1/112^\circ$ spatial resolution (i.e. approximately $700 \text{ m} \times 1000 \text{ m}$) over the study area, whereas the native size of VEGETATION pixels is 1 km^2 .

The minimal number of instantaneous VEGETATION data (NMOD) used to estimate the 10-day reflectance was 3. As a consequence, when NMOD was under this threshold the 10-day observation was not provided. The combination of daily data coming from both sensors VEGETATION 1 and VEGETATION 2 when available increased NMOD. This was useful for improving the quality of the directional normalisation and for limiting the amount of missing data. The combination of VEGETATION 1 and 2 images occurred only in 2003 for the whole year, in 2002 after June 1, and in 2004 before April 1. VEGETATION 1, exclusively, was used before June 1, 2002 while VEGETATION 2, exclusively, was used after April 1, 2004. All yearly time-series were incomplete except for 2003 due to the cloud or the snow cover during winter and spring especially in mountains. Thus, the dataset includes both spatial and temporal gaps. The gaps were the largest before and during the leaf unfolding period and less marked during senescence. For instance, over the whole study area there were no missing data only for a small number of 10-day periods: 10 periods in 2002, 4 in 2003, 1 in 2004, 6 in 2005, and 3 in 2006. These 10-day periods only occurred in July, August, September and October. These numerous gaps in the time-series could lead to large errors in the detection of the different phenology stages each year. For instance, Zhang et al. (2009) showed that, using the 16-day MODIS products, two consecutive missing data during the phenophases of interest can multiply by 5 the risk of detection error larger than 5 days in comparison with only one missing data. Some algorithms exist to fill spatio-temporal gaps. But they are based on smoothing techniques (e.g. Gao et al. 2008) and in the case of large gaps they are not able to accurately reconstitute the annual kinetics of the remote sensing signal and its spatial variability. In addition, the algorithm we used for unmixing this kinetics required the temporal continuity of the data. Therefore, as our study was focused on the analysis of the elevation variations in phenology and not on its interannual changes, we pooled the data from the five years to build a sole mean year, assuming the interannual variations in the vegetation seasonal dynamics during the five-year period were lower than the variations due to changes in the elevation over the whole region. This later assumption was supported by the *in situ* measurements obtained by Vitasse et al. (2009a,b) (Cf Fig. 3a for oak and beech trees). A pixel was thus retained if its NMOD was larger than 2 at least once during the five years (2002–2006) for each 10-day period. In order to minimise the number of rejected pixels, the study period was reduced; it was determined as March 11 to November 11, which spans the whole part of the potential growing season. After this data processing, 12686 pixels were selected. The removed pixels were mostly located at an elevation greater than 1800 m corresponding to the tree line of broadleaf forest.

The unmixing statistical model of Cardot et al. (2008) we used in this study required the remote sensing response of the pixel to be a linear combination of the responses of the sub-pixel components. The ratio-based indices commonly used in phenology studies such as NDVI (normalised vegetation index) or EVI (enhanced vegetation index; Huete et al., 2002) are not compatible with this constraint. Conversely, indices such as the DVI (Difference vegetation index) or PVI (Perpendicular Vegetation Index) are linear indices (i.e. computed from a linear combination of the measured reflectance observations) and they contain more information about the vegetation dynamics than the NDVI (higher Signal to Noise Ratio (Maignan et al. 2008), less saturation problems (Huete et al. 2002), etc.). We chose to use the PVI index which has been designed to minimize its sensitivity to soil reflectance (Richardson & Wiegand, 1977). The PVI is a linear combination of the red (RED) and near infrared (NIR) reflectances: $PVI = (NIR - aRED - b) / \sqrt{1 + a^2}$ where a and b are respectively the slope and the intercept of the soil line. The soil line equation was approximated from a linear regression of the NIR reflectance as a function of RED reflectance over non-vegetated surfaces. As too few VEGETATION data were available over pure agricultural areas in winter when the soil is bare, we used the observations made over pure bare rock pixels in July and August. The linear regression was performed on the 10-day reflectances after averaging the observations over the 5 years. A significant linear relationship between NIR and RED reflectances was obtained ($n = 312$, $r^2 = 0.47$, p -value of t -statistics for the parameters a and b was < 0.0001), with $a = 0.757$ (standard error = 0.023) and $b = 0.077$ (0.002). It resulted that $PVI = 0.797NIR - 0.604RED - 0.06$.

2.4. Unmixing of the seasonal variations in PVI

The unmixing methods were initially developed to estimate the sub-pixel land use composition (Foody & Cox, 1994). Recently, the model of Cardot et al. (2008) dealt with the inverse problem to retrieve the seasonal variations in the remote sensing signal of each land use in each pixel given that the within-pixel land use is known. Due to its large size – nearly 1 km^2 – the VEGETATION pixel generally includes several land uses. As a consequence, the PVI computed from the VEGETATION observations can be assumed to be a linear combination of the PVI values specific to each land use element. The reflectance variability of a given land use within a pixel being assumed relatively small compared to the variability between pixels, the PVI observed by VEGETATION over the pixel i as function of time (t) i.e. $X_i(t)$ was modelled as:

$$\begin{cases} X_i(t) = \sum_{j=1}^J \pi_{ij} \rho_{ij}(t) + \varepsilon_i(t) & t \in \{t_1, \dots, t_p\} \\ \rho_{ij} \sim \mathcal{N}(\rho_j, \Gamma_j), j = 1, \dots, J \end{cases} \quad (1)$$

where

i	index for pixel
t	time, i.e. the 10-day period
p	number of 10-day periods
J	number of the land use classes
j	index for land use class
$X_i(t)$	PVI of the pixel i observed from VEGETATION over the 10-day period t
π_{ij}	area fraction of the land use j within the pixel i , with $\sum_j \pi_{ij} = 1$
$\rho_{ij}(t)$	PVI of the land use j within the pixel i at the 10-day period t
$\rho_j(t)$	Expectation of the random function $\rho_{ij}(t)$ for the land use j at the 10-day period t

$\varepsilon_i(t)$ error, assumed independent and Gaussian
 Γ_j temporal covariance matrix with the following elements:

$$[\Gamma_j]_{l,l'} = \text{cov}(\rho_{ij}(t_l), \rho_{ij}(t_{l'})), l, l' = 1, \dots, p.$$

Therefore the estimation of the PVI seasonal variation ($\rho_{ij}(t)$) of each land use class j present in each pixel i was performed assuming the surface fraction of each land use j (π_{ij}) within the pixel i was known. This unmixing (or disaggregation) of $X_i(t)$ was based on the varying-time random effects regression model proposed by Cardot et al. (2008). Introducing random effects allows us to estimate individual variations in PVI, i.e. between pixels.

The estimation method is detailed in Cardot et al. (2008). First, given that π_{ij} is known $\rho_j(t)$, and Γ_j are estimated from the observed PVI ($X_i(t)$) and their temporal covariance ($\text{cov}(X_i(t_l), X_i(t_{l'}))$) by maximizing the likelihood. Each individual response $\rho_{ij}(t)$ is then predicted using the Best Linear Unbiased Prediction (BLUP) formula. The two steps include an approximation to the seasonal curves of $\rho_j(t)$ and $\rho_{ij}(t)$ with B-Splines functions, which reduces the number of parameters to be estimated and smoothes the produced curves. Finally, this statistical approach produces non-parametric models of the seasonal variation in PVI, since it is based on the explicit use of the temporal covariance between numerous VEGETATION observations, without any prior knowledge of the biological and physical determinism of the seasonal variations in PVI.

The area fraction of each land use within each pixel (π_{ij}) was provided by the seamless vector data of European CLC2000 geographical database, which describes the land use in 2000 with forty-

four classes and with a minimal mapping unit equal to 25 hectares (EEA, 2000). About twenty classes of land use were represented in the study area. The forest ecosystems belonged to three broad classes, which were kept in their original states: “Deciduous broadleaf forest”, “Coniferous forest”, and “Mixed forest”. The non forested CLC2000 classes were pooled together to form 2 large classes. The first class, named “No or Sparse Vegetation”, pooled artificial areas (urban, industrial) and natural non or sparsely vegetated surfaces. Pixels including water bodies were discarded from the data set. The second, named “Agricultural Surfaces”, pooled the non-forest vegetation classes, mainly composed of crops, pastures, and natural grasslands. Our main land use of interest, i.e. the deciduous broadleaf forests, was present in ~70% of the studied pixels, with $\pi_{ij=\text{deciduous}}$ varying from less than 1% to 100%.

The algorithm was applied to the observed PVI of the mean year ($X_i(t)$) made up of 25 successive 10-day periods from March 11 to November 11; i.e. for time t varying between DOY 70 and 315 every 10 days. The used B-Splines functions were parameterized with their order (q) and the number (k) of interior knots evenly spaced within the period of interest. These were the same for $\rho_j(t)$ and $\rho_{ij}(t)$. Some tests were made with the value range indicated by Cardot et al. (2008) in order to maximise the modelling accuracy and optimise the number of land use classes to be used. Thus, in the case of the land use distribution into the five classes previously described (i.e. $J=5$), q and k were defined as follows: $q=3$, $k=5$.

In the following, the modelled $\rho_{ij}(t)$ and $\rho_j(t)$ will refer to as, respectively, the individual seasonal (or phenological) response of PVI at a pixel i level, and to the mean seasonal (or phenological) response for a given land use j . The 10-day periods will be labelled with the date of their first day.

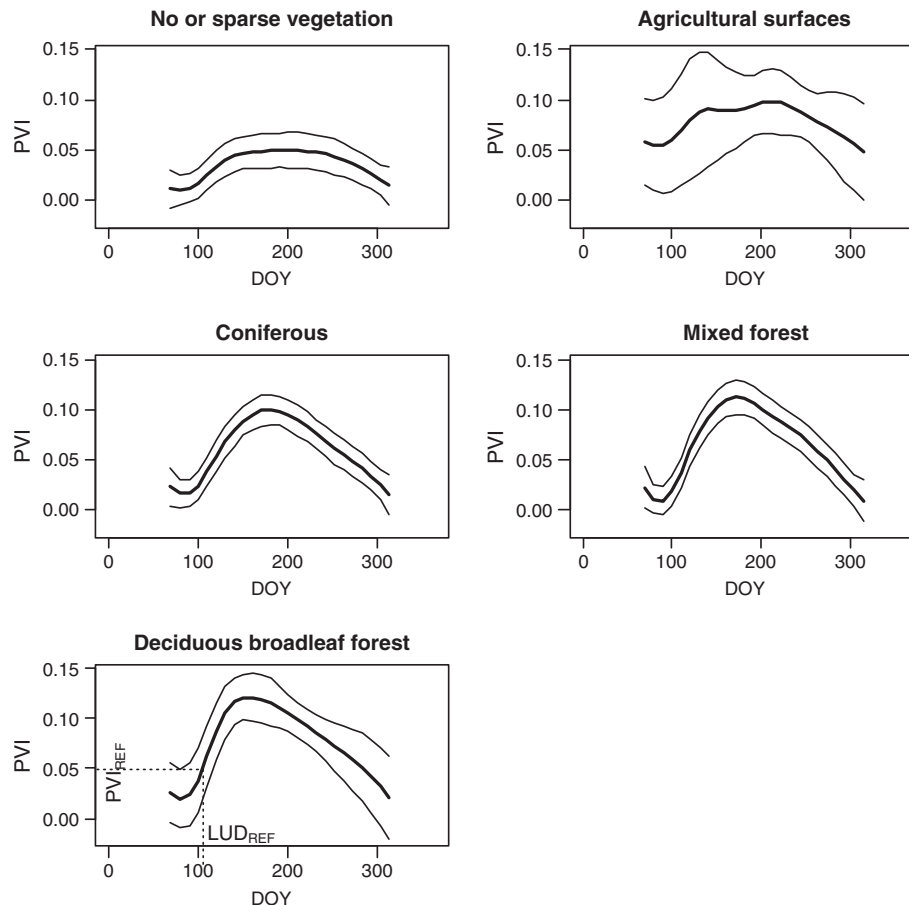


Fig. 4. Seasonal variations in mean PVI estimated for each land use class ($\rho_j(t)$) from the Cardot's model. Thin lines correspond to ± 2 instantaneous standard deviation. Plot for the deciduous broadleaf forest: the dotted lines indicate LUD_{REF} ($= 105.5$) and the corresponding value of PVI ($= PVI_{REF}$).

2.5. Characterising elevation variations in the PVI seasonal response of deciduous broadleaf forest

The mean elevation of each VEGETATION pixel (cf. Fig. 1) was estimated by aggregating the Shuttle Radar Topography Mission data at 90 m resolution (USGS, 2005). The relationship between elevation and the PVI seasonal signature of the deciduous broadleaf forests was investigated in two complementary ways. First, we examined the spatial variations in the PVI individual seasonal signatures of broadleaf forests (i.e. $\rho_{ij=deciduous}(t)$). The pixels containing deciduous forests were then partitioned into several seasonal curve classes applying the K-means clustering algorithm of Hartigan & Wong (1979). After some tests, the number of classes was empirically fixed as being eight in order to best express the variability of the temporal behaviour of PVI. The distribution of elevation within and between each produced class was then investigated. Second, we compared the variations between the PVI individual seasonal responses averaged by 100 m wide elevation class.

2.6. Leaf unfolding dating

Cardot's model does not produce any parametric function of PVI as a function of time. Moreover, because of the very high temporal autocorrelation of PVI induced by the unmixing process, the parametric regression methods were not well suited to model the PVI versus time in order to estimate the critical dates of PVI seasonal changes. Furthermore, as the unmixing provided an estimate of the PVI of the set of all deciduous broadleaf stands included in each pixel (i.e. $\rho_{ij=deciduous}(t)$), the PVI of each tree population observed at the ground could not be distinguished and $\rho_{ij=deciduous}(t)$ could not be compared directly with the local ground-based phenology observations. For these reasons, the LUD of broadleaf forests was retrieved from the VEGETATION observations using the following two steps.

First, over each pixel i , an earliness index IE_i was calculated. It was designed to be an index estimating the advance ($IE_i < LUD_{REF}$) or the delay ($IE_i > LUD_{REF}$) in leafing over each pixel in comparison with the ground-based mean date of leaf unfolding (LUD_{REF}). PVI_{REF} denoted the value of the mean PVI ($\rho_{j=deciduous}(t)$) on the day of year = LUD_{REF} (see Fig. 4). For each pixel i containing broadleaf forests, IE_i was defined as the date at which the individual PVI ($\rho_{ij=deciduous}(t)$) was equal to PVI_{REF} : $\rho_{ij=deciduous}(IE_i) = \rho_{j=deciduous}(LUD_{REF}) = PVI_{REF}$.

PVI_{REF} was estimated by linear interpolation of $\rho_{j=deciduous}(t)$ between the two closest 10-day periods surrounding LUD_{REF} . IE_i was estimated from a linear interpolation of $\rho_{ij=deciduous}(t)$ within the 10-day interval including the PVI_{REF} value.

In a second step, the elevation variations in IE_i , computed from the VEGETATION observations, were evaluated by comparing with the ground-based observations of LUD. As discussed above, a direct comparison between the retrieved satellite data at pixel level and the local *in situ* data could not be made. Therefore, this comparison was made using averaged values of IE_i by 100 m wide class of elevation. The ground-based mean LUD in each elevation class was given by LUD_d (Cf. Section 2.2, Fig. 3b). The equation linking the two variables was then statistically calibrated by linear regression. It was applied over each studied pixel to calculate $SLUD_i$, i.e. the satellite-based leaf unfolding date. Lastly a $SLUD$ map was produced over the whole study area.

3. Results

3.1. PVI seasonal response of the various land uses

The mean phenological PVI curves obtained for each land use class ($\rho_j(t)$) and the variability (± 2 standard deviation) of the estimated individual PVI are shown in Fig. 4. The seasonal variations of "No or sparse vegetation" were very weak. Conversely, "Deciduous broadleaf forest", "Agriculture surfaces", and "Mixed forest" showed the highest

amplitudes during the year. The greatest variability of PVI individual values was observed with the two former classes. It was maximal for the "Agricultural surfaces" class, which regroups various crops and grasslands with different seasonal leaf area cycles due to species and crop calendars diversity. The mean curve for broadleaf forests is realistic and consistent with ground observations: a minimum and maximum, occurring respectively in March (DOY=80) and in June (DOY=162), was in agreement with the time interval of the oak and beech flushing (from DOY 80 to 150, Fig. 3). The individual PVI variability was maximal during the transitional periods of foliar phenology: at the end of winter and the beginning of spring, when the annual growth cycle of leaves started again, and in fall, when the cycle finished with senescence, i.e. yellowing and falling of leaves. A lower dynamics throughout the year can be seen for the coniferous forests, where non deciduous species were dominant.

3.2. Accuracy in the unmixed PVI seasonal response of deciduous broadleaf forest

Fig. 5 shows the distribution of errors on the modelled individual responses and their seasonal variations for the pixels containing broadleaf forests. These are the residuals between the observed PVI ($X_i(t)$) and the modelled PVI ($\sum_{j=1}^J \pi_{ij} \rho_{ij}(t)$). The errors were minimal

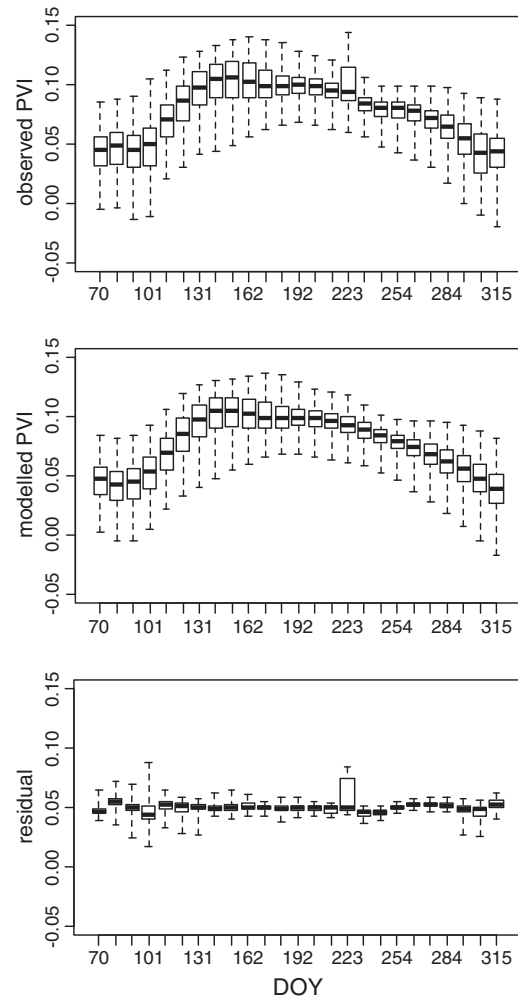


Fig. 5. Distribution of errors in the modelled PVI at pixel level of the land use classes set from Cardot's model. Results are given only for pixels containing deciduous broadleaf forest ($\pi_{ij=deciduous} > 0$). Observed PVI = $X_i(t)$, Modelled PVI = $\sum_{j=1}^J \pi_{ij} \rho_{ij}(t)$, Residual = Observed - Modelled. Definition of $X_i(t)$, π_{ij} , $\rho_{ij}(t)$: see Eq. (1). Boxes and bars give the quantiles 1, 25, 50, 75 and 99.

when the number of PVI data per 10-day period used to calculate the mean year is maximal, i.e. when NMODR which is the number of times when $NMOD > 2$ equalled 5. This was the case from DOY 141 to DOY 284 except on DOY 223. It is likely that the isolated very high errors obtained for DOY 223 could be attributed to an insufficient filtering of pixels contaminated by clouds in 2006. Nevertheless, the largest errors occurred mainly before DOY 141, when many data were missing, especially in 2004 and 2005, due to clouds and snow. Thus, at the end of winter and at the beginning of spring, NMODR was often less than 5 and the index of quality NMOD was often lower than for the rest of the year. Finally, we can consider that the unmixing smoothed the impact of erroneous values of instantaneous PVI due to cloud or snow effects and reduced the noise induced by missing data.

The accuracy of PVI individual seasonal responses estimates ($\rho_{ij=deciduous}(t)$) of broadleaf forests seems to depend strongly on their proportion ($\pi_{ij=deciduous}$) within the pixel. As shown in Fig. 6, the smaller $\pi_{ij=deciduous}$, the smaller the deviation of the individual PVI from the mean response of the land use class ($\rho_{j=deciduous}(t)$), namely, the PVI signature of the deciduous fraction within the pixel became identical to the mean PVI response of deciduous forests, computed over the whole study area. The deviation was almost equal to zero when $\pi_{ij=deciduous}$ was smaller than 10%. This underestimation of the individual effect – in absolute value – was found to be very significant when $\pi_{ij=deciduous}$ was lower than approximately 40% (Cf Fig. 6). Consequently, we assumed in this study that the estimates of PVI individual seasonal responses of deciduous forests were not satisfactory as long as $\pi_{ij=deciduous}$ was lower than 40%. In the following, only the pixels exceeding this threshold of 40% will be analysed. The latter

represented 3183 pixels over the 8975 pixels containing broadleaf forests; approximately 20 times more than the 139 pure pixels (cf. Table 1) which would be studied if unmixing was not used. These 3183 pixels provided a large sampling of the elevation range from 0 to 1700 m over the Pyrénées study area (Table 1).

3.3. Effect of elevation on the PVI seasonal response of deciduous broadleaf forest

The K-means classification over the deciduous forests led to pool the individual seasonal curves $\rho_{ij=deciduous}(t)$ of similar shape (Fig. 7). The eight obtained classes showed various seasonal patterns of PVI (Fig. 7b), which appeared to depend mainly on elevation (Fig. 7c). Their spatial distribution also exhibited a patchy structure which seems to reflect the relief pattern (Fig. 7a). Therefore, the classes with the lowest PVI at the beginning and at the end of the annual cycle (classes 1 to 4) could be found mostly in the southern part of the study area at the highest elevations (approximately >500 m) and their seasonal amplitude was the greatest. Conversely, K-means classes with the highest PVI values at the onset and at the end of the year (classes 5 to 8) were located in the plain or hilly area (approximately <500 m) in the northern part of the study area. The date at which the maximal PVI was reached increased as elevation increased. The PVI seasonal pattern was found to be more sensitive to elevation (Fig. 7c) within the group of classes 1 to 4, i.e. for elevation >500 m, than within the other group (classes 5 to 8) at lower elevation. However, the gradation of the eight PVI curves within each group over the whole annual cycle, given in Fig. 7b, was not in close agreement with

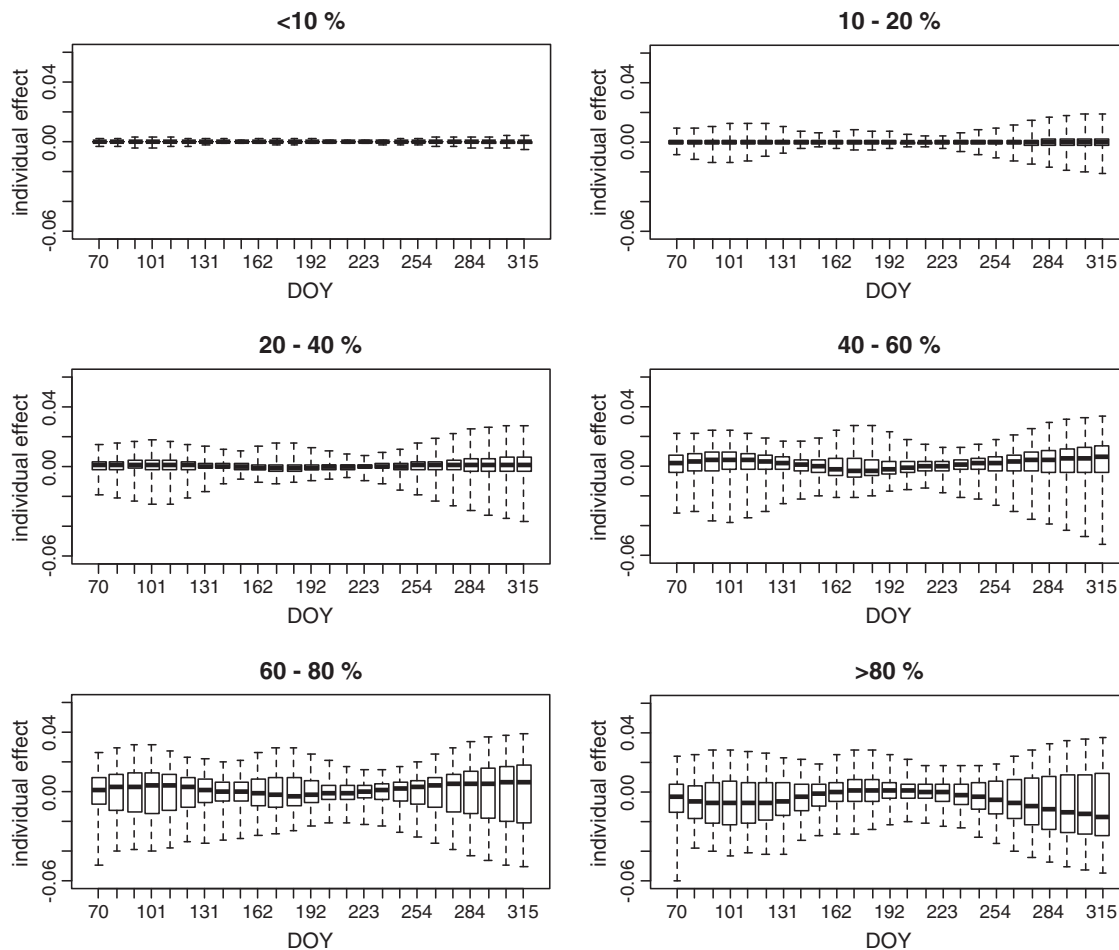


Fig. 6. Deviations between individual ($\rho_{ij=deciduous}(t)$) and mean ($\rho_{j=deciduous}(t)$) PVI of deciduous broadleaf forest, estimated from Cardot's model, as a function of the fraction of broadleaf forest $\pi_{ij=deciduous}$ in the pixel. Boxes and bars give the quantiles 1, 25, 50, 75 and 99.

Table 1

Characteristics of pixels including deciduous broadleaf forest as a function of elevation. The cloudy or snowy pixels and those with fraction of deciduous broadleaf forests $\pi_{ij=deciduous} < 40\%$ were not taken into account.

Elevation classe	Elevation range (m)	Mean elevation (m)	Mean $\pi_{ij=deciduous}$ (%)	Pixels number
<i>(a) pixels with $\pi_{ij=deciduous} > 40\%$, $n = 3183$</i>				
0	0–100	65	55	152
1	100–200	148	57	481
2	200–300	249	58	735
3	300–400	344	61	458
4	400–500	445	63	309
5	500–600	548	63	182
6	600–700	647	67	148
7	700–800	751	72	134
8	800–900	850	75	123
9	900–1000	945	75	124
10	1000–1100	1046	76	112
11	1100–1200	1148	76	78
12	1200–1300	1251	75	75
13	1300–1400	1343	68	50
14	1400–1500	1429	64	14
15	1500–1600	1554	52	6
16	1600–1700	1626	46	2
<i>(b) pure pixels ($\pi_{ij=deciduous} = 100\%$), $n = 135$</i>				
0	0–100			0
1	100–200	138	100	4
2	200–300	256	100	14
3	300–400	351	100	8
4	400–500	438	100	5
5	500–600	548	100	7
6	600–700	651	100	9
7	700–800	754	100	19
8	800–900	850	100	12
9	900–1000	939	100	19
10	1000–1100	1038	100	19
11	1100–1200	1149	100	10
12	1200–1300	1244	100	10
13	1300–1400	1368	100	3
14	1400–1500			0
15	1500–1600			0
16	1600–1700			0

that of elevation. It also depended on the area fraction covered by deciduous as shown in Fig. 7d. In addition, an analysis of variance (one-way ANOVA) showed elevation and $\pi_{ij=deciduous}$ were significantly different between the eight PVI signature classes with F-statistics equal respectively to 788.4 and 88.4, i.e. p -value < 0.0001 for degree of freedom = 7 for both variables. In addition, a multiple comparison of means (paired t-tests with Bonferroni correction) showed there was a significant difference (p -value < 0.001) between all K-means classes in mean elevation, except between classes 2 and 3, 5 and 7, 6 and 8, and in mean $\pi_{ij=deciduous}$, except between classes 1 and 3, 2 and 4, 2 and 8, 4 and 8, 6 and 7.

Furthermore, when the PVI individual curves were averaged by 100 m wide class of elevation (Fig. not shown, results are similar to those given in Fig. 7b), it was found that the seasonal course of PVI changed progressively with elevation increase. For instance, as elevation increases, we note a decrease in PVI at the beginning and the end of the vegetation cycle (black arrows in Fig. 7b) and a shift in the peak of maximal PVI from the spring end towards the summer onset with shortening of the duration of high PVI values (white arrows in Fig. 7b). The weaker sensitivity of the PVI seasonal course to elevation for elevation lower than 500 m was confirmed. The PVI curves of the five lowest altitude classes (< 500 m) are very close before DOY 125 (i.e. before budburst) and almost identical at the end of the fall during the phase of foliage senescence (after DOY 200). During the phase of green-up in spring (between DOY 80 and DOY 162), the time delay in the PVI spring increase happens without change in slope when mean elevation decreased from 1700 m to 500 m. Below 500 m, during the same phase, the slope of PVI as a

function of time was slightly reduced with elevation decrease and it was minimal for elevation lower than 100 m.

3.4. Leaf unfolding date

The PVI_{REF} , i.e. the value of mean PVI for the mean date of leaf unfolding LUD_{REF} (= 105.5) was equal to 0.0485. A strong linear relationship was found between IE, i.e. the date when individual PVI reached PVI_{REF} , and LUD, i.e. the ground-based leaf unfolding date – which were both averaged by 100 m wide class of elevation (Fig. 8). Moreover, no difference was found when taking into account either mixed or pure pixels. The RMSE (root mean square error) of the mean LUD predicted from the mean IE for each 100 m wide elevation class by using regression models calculated over pixels with $\pi_{ij=deciduous} > 40\%$ and over only pure pixels were similar and equal to approximately 2 days (1.8 and 2.1 days respectively). The mean bias was close to zero in both cases. However, for $\pi_{ij=deciduous} > 40\%$ the slope of IE as a function of LUD was lower for $LUD < 110$, i.e. for forests located at elevation < 500 m, than for $LUD > 110$ (Fig. 8). In order to reduce possible errors due to the unmixing method, the equation of regression fitted over pure pixels was applied to each individual value of IE to compute the satellite-based estimates of LUD (SLUD), which is given by $SLUD = 1.83 IE - 82.7$. This estimation was not possible for a few pixels whose PVI was always greater than PVI_{REF} in spring. Fig. 9 shows the variations in SLUD as a function of the elevation for $\pi_{ij=deciduous} > 40\%$ and for pure pixels. SLUD averaged by 100 m wide class of elevation seemed globally consistent with the elevation pattern of LUD estimated from the field observations. In addition, the individual SLUD values are distributed more or less symmetrically around this ground-based pattern. However, for $\pi_{ij=deciduous} > 40\%$, when the elevation is smaller than 500 m, SLUD appears to be slightly overestimated: many retrieved values are concentrated near DOY 105 and the SLUD values averaged by elevation class have an elevation variation lower than the ground-based LUD. These effects were clearly attenuated for $\pi_{ij=deciduous} > 60\%$ (not shown) and disappeared for pure pixels. Whatever the elevation, the dispersion of individual values of SLUD was very large, approximately ± 20 days. The spatial pattern of SLUD is shown in Fig. 10. The impact of the relief can be clearly seen for forests in mountains, with SLUD varying mainly between DOY 115 and 140 (i.e. from 25 April to 30 May) similarly to *in situ* observations. In the forests of plain, hill or piedmont SLUD showed a clear spatial pattern. It spanned the large range of values – approximately from DOY 85 to 115 (i.e. from 25 March to 25 April) – measured at ground level on beech and oak populations.

4. Discussion

4.1. Remote sensing time-series

All results presented in this study are based on the analysis of the seasonal variability of the five-year average PVI vegetation index derived from VEGETATION data measured during 5 successive years from 2002 to 2006. The building of an averaged 2002–2006 year allowed us to fill the large temporal gaps in the VEGETATION time-series due to cloud and snow presence – frequent in mountains – at the end of winter and at the beginning of spring, i.e. the period of green-up of deciduous forests. Methods based on a spatio-temporal smoothing of data year by year (e.g. Gao et al., 2008), or on the use of a compositing interval wider than 10 days could not provide satisfactory results (Robin et al., 2008), since they would limit capabilities to detect gradual changes in green leaf area due to leaf flushing and to date accurately leaf unfolding. Aggregating the pixels also could not be a suitable solution. In mountains, the coarse resolution pixel, for instance with the global 8 km AVHRR data often used at continental scale, includes a range of elevation which is too large to capture accurately the interannual changes in phenology of broadleaf forests (Maignan et al., 2008). The number of available VEGETATION data

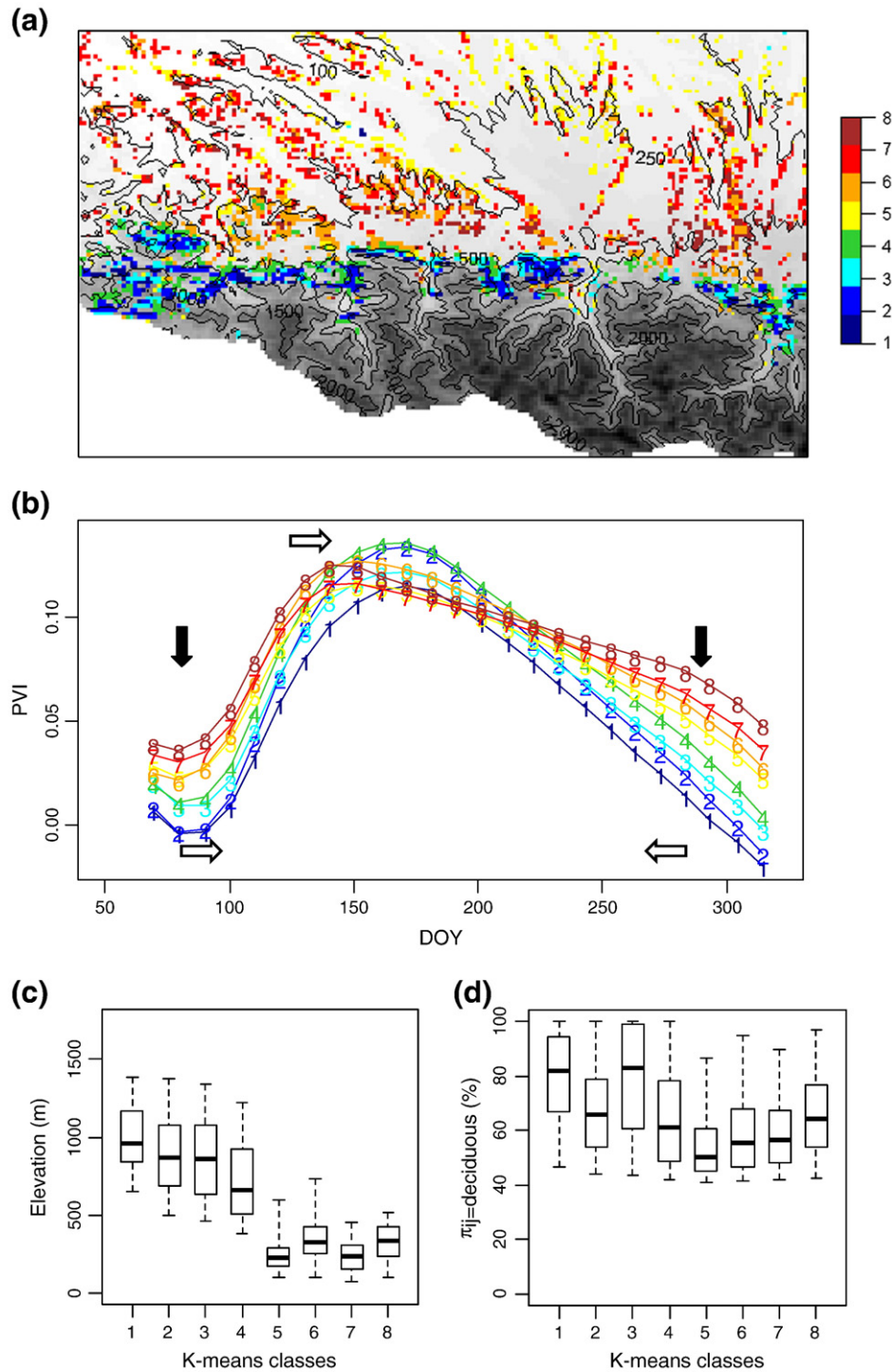


Fig. 7. Variations in individual PVI seasonal curves of deciduous broadleaf forest summarised from a K-means classification applied over pixels with fraction of broadleaf forest $\pi_{ij=deciduous} > 40\%$ ($n=3183$): (a) Map of the eight classes of curves. Background: elevation in grey tones with isolines (100, 250, 500, 1000, 1500, and 2000 m) (b) Curves of centres of classes. Arrows symbolise the main effects of elevation increase (c) Distribution of the mean elevation of the pixels within each class (quantiles: 5, 25, 50, 75, and 95 in both boxplots) (d) Distribution of $\pi_{ij=deciduous}$ of pixels within each class (quantiles: 5, 25, 50, 75, and 95 in both boxplots).

per 10-day period for each selected pixel was variable in spring during the 2002–2006 period: varying from 1 to 5. This might have a strong impact on the estimates of the 5-year mean PVI. However, the resulting noise seemed to have been smoothed by the Cardot's algorithm, as suggested by the seasonal distribution of errors between modelled and observed data averaged over the five years (cf. Fig. 5). Finally, although averaging the VEGETATION data over five years into a single representative year led to a loss in information about the interannual variability of

leaf phenology, this approach made it possible to investigate the elevation variations in the seasonal remote sensing response over a large range of elevation (0–1700 m) and over a very short range of latitude (approximately 1°) covering a relatively small area.

As measurements of the reflectance of soil under the forest canopy of the study area were unavailable, the parameters of the soil line equation were estimated from the VEGETATION data on pure pixels of bare rock in summer. Their values were close to those estimated in

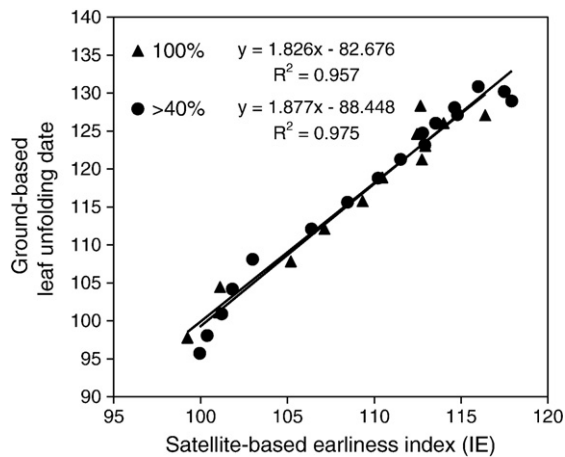


Fig. 8. Linear regression between satellite-derived earliness index (IE) and ground-based leaf unfolding date (LUD). Both are averaged by 100 m wide elevation class. Results for pixels with a fraction of deciduous broadleaf forest $\pi_{ij=deciduous}>40\%$ and for pure pixels (100%). RMSE is equal to 1.8 and 2.1 days, respectively.

winter from the same VEGETATION time-series on pure pixels of maize crops located on the sandy soils of South-West France (Guyon et al., 2006). In both cases the slope of the soil line was smaller than unity (0.757 for the bare rock, 0.883 for the sandy soils). The use of these soil line equations could lead to overestimate the contribution of NIR in the PVI formula compared to that estimated from ground

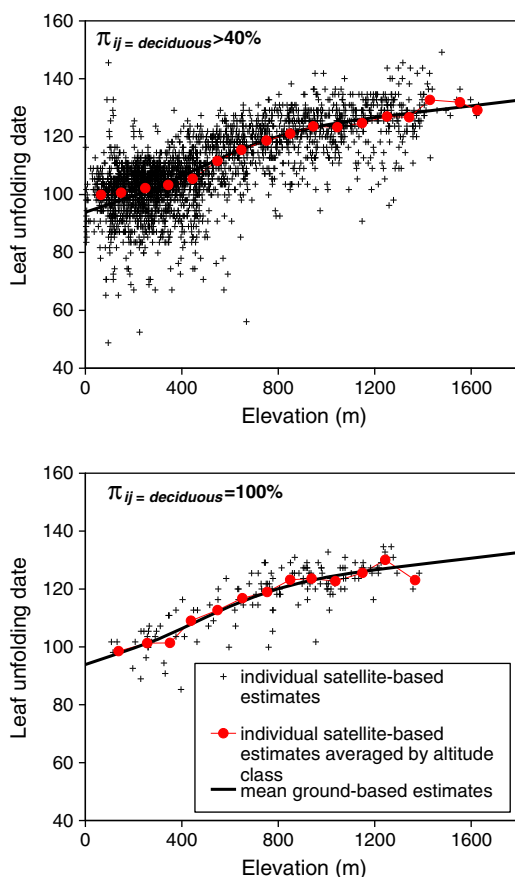


Fig. 9. Satellite-based date of leaf unfolding (SLUD) as a function of elevation for pixels with fraction of deciduous broadleaf forest $\pi_{ij=deciduous}>40\%$ ($n = 3183$), and $=100\%$ ($n = 135$), in comparison with the elevation pattern of the mean ground-based LUD (namely LUDd). Individual SLUD values are indicated by crosses. Their average by 100 m wide class of elevation is superimposed in red. The satellite-based estimates result from the application of the linear model shown in Fig. 8 fitted on broadleaf pure pixels ($\pi_{ij=deciduous} = 100\%$).

measurements over various soil types (whose slope has been found to be always greater than unity (Gilbert et al., 2002; Rondeaux et al., 1996)). Nevertheless, possible errors in the estimation of PVI should be not critical in our study, since the calculation of the soil line equation was made from the same dataset, i.e. with the same spectral sensitivity and with the same radiometric processing.

The Cardot's method was used to unmix the seasonal radiometric response of each land use class present within each 1-km² pixels. It allowed us to assess the elevation variations in the phenological behaviour specific to the deciduous broadleaf forests, even though this land use class pooled several tree species and various forest types. Thus, all pixels which spanned the whole elevation range (from 0 to 1700 m) of the deciduous forests in the study area could be analysed. Using only pure pixels ($n = 139$), a more restricted range of elevation (from 100 to 1300 m) could be explored because of the fragmentation of the forests at a scale of 1-km² pixel. Nevertheless, the individual response of broadleaf forests could not be accurately unmixed for pixels when the area fraction of this forest type is a too low ($<20\%$).

4.2. Retrieving the seasonal dynamics of deciduous broadleaf forest

The retrieved seasonal dynamics of the PVI vegetation index is consistent with the seasonal changes in the green leaf area expected over the study area. As expected, seasonal variations in PVI were stronger for deciduous broadleaf forests than for forests including evergreen species (i.e. coniferous). The elevation gradient of temperature explains a large part of the spatial distribution of the PVI phenological responses of the deciduous forests. Shortening of the vegetative season length through elevation was revealed in the delay of the PVI increase in spring and the advance of its decrease in fall, as observed by Beck et al. (2008) for seasonal trajectory of NDVI of deciduous and mixed forests ranging from 1000 to 2900 m in China. The decrease in PVI in autumn was more variable than its increase in spring (as shown in Fig. 7b). This could attest the complexity of the determinism of processes of yellowing and falling of foliage compared to the leafing ones. For instance Vitasse et al. (2009b) found no correlation between senescence and air temperature for ash (*Fraxinus excelsior*) and sycamore maple (*Acer pseudoplataneus*). Plain and hill forests showed phenological patterns quite different from mountainous ones, particularly with a greater earliness of maximum PVI which is likely to be due to the earlier growth of leaves. Other factors related or not to elevation contribute to enhance the patchy pattern of the spatial distribution of PVI phenological responses, such as the elevation or geographic range of tree species which differ in their phenology sensitivity to temperature. It is likely the elevation range of species led to accentuate the difference between mountain and low-lying areas since the pure forests of beech were more frequent in mountains. Conversely, for elevations lower than 500 m, the sensitivity of PVI phenology to the elevation gradient of temperature was most likely attenuated by the geographic pattern of species. At low elevation, the pure forests of sessile oak and the forests containing various deciduous species (such as ash and beech) with different phenological properties (Vitasse et al., 2009a,b) were not located in the same areas. The effect of the within-pixel fraction of deciduous forest over the PVI seasonal course, shown in Fig. 7d and by the ANOVA tests, could be an artefact due to the unmixing method. However it could also express the high heterogeneity in species composition of the very fragmented forests of the study area. Lastly, the understory vegetation plays certainly a central role in the seasonal course of reflectance of forest stands (Rautiainen et al., 2009). Its impact should be considered in the analysis, especially for forest types where the undergrowth species leaf out before the tree layer ones (Ahl et al., 2006). Nevertheless, our results were consistent with those of Vitasse et al. (2009a) based on ground observations, which showed that the timing of leaf unfolding of trees is mostly determined by

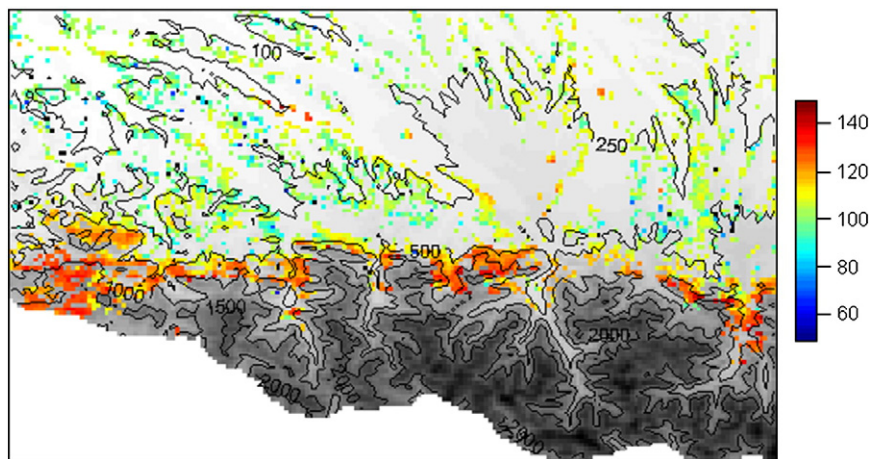


Fig. 10. Spatial variations in the individual satellite-based dates of leaf unfolding (SLUD) for pixels with fraction of broadleaf forest $\pi_{ij=deciduous} > 40\%$ ($n = 3183$). The estimates result from the application of the linear model shown in Fig. 8 fitted on broadleaf pure pixels ($\pi_{ij=deciduous} = 100\%$). Background: elevation in grey tones with isolines (100, 250, 500, 1000, 1500, and 2000 m). Black: pixels where no estimation was possible ($n = 28$).

spring temperature and its altitudinal gradient and that it strongly differed among species.

4.3. Satellite-based estimates of elevation variations in leaf unfolding date

The elevation variations in satellite-based estimates of leaf unfolding date (SLUD) averaged by 100 m wide class of elevation agree with the mean elevation pattern of LUD observed at the ground (LUDd), although the latter was calculated by assuming the deciduous forests are composed only of sessile oak and beech. They reproduced quite well the mean delay of approximately 2.3 days for each 100 m elevation increase over the whole elevation range (0 to 1700 m). Nevertheless for low elevations (<500 m) the sensitivity of SLUD to elevation was lower than the expected one: the mean delay was approximately 1.5 days 100 m^{-1} . It is likely this was due to the presence of species different from beech and oak, and also, to the inaccuracy of the unmixed PVI response in the pixels including a low fraction of deciduous forest. In addition, the expected estimation error of SLUD for a given elevation was approximately 2 days (cf. Fig. 8). This accuracy can be considered as satisfactory since it would allow us to detect changes in leafing timing of deciduous broadleaf forests with a magnitude equivalent to that due to an elevation variation of 100 m (2.3 days on average), or in other words, to that caused by a variation in the mean annual air temperature of 0.5 °C. These results make us confident in the robustness of the mean leaf unfolding dates estimated per 100 m wide class of elevation from the VEGETATION time-series averaged on five successive years to monitor the long-term trends under the climate change.

The estimation of the leaf unfolding date at pixel level was likely to be less accurate. The variability of the estimates for a given elevation is high, i.e. approximately ± 20 days around the mean elevation pattern (Fig. 9). This variability seems to be not too excessive in comparison with the one observed at ground level between tree populations of all species (cf. Fig. 3, Vitasse et al., 2009b). Some possible sources of variability can be mentioned. The impact of the species composition (Fisher et al., 2007), of the frequency and mixture of species present within each pixel (Badeck et al., 2004) and of the errors due to the unmixing method have already been discussed. The possible effect of elevation variations within each pixel (cf. Maignan et al., 2008) can be assumed to be as relatively low: the within-pixel standard error of elevation is lower than 190 m over all pixels containing deciduous forests and is lower than 39 m for 75% of these pixels. Other sources of variability in the leaf unfolding date at pixel level are the microclimatic conditions which have an influence on air temperatures (Fisher

et al., 2006), changes in land use, silvicultural or accidental forest changes due for instance to timber felling or fire, uncertainties in the pixel geolocation, etc. In addition, the compositing of VEGETATION data by 10-days intervals and their normalisation of directional effects on large periods (up to 30 days) could also bring a significant part of uncertainty on the dating, as the distribution of acquisition dates of images used for estimating the reflectance value assigned to each ten-day period varied between pixels (Thayn & Price, 2008). However, the averaging of the VEGETATION data over five years could attenuate partly these different effects. A strong consistency in the spatial pattern of the leaf unfolding dates can be seen in the map given in Fig. 10, which makes us confident in the quality of the remotely sensed retrievals at pixel level.

4.4. Interactions between phenology and disturbances in the seasonal remote sensing signal

As previously mentioned, monitoring of leaf phenology and of its changes due to climate forcing from satellite observations could be affected by some seasonal changes in the reflectance resulting from natural environmental factors or accidental events, (e.g. snowmelt, drought, forest fires) or from anthropogenic activities (e.g. land use change, timber felling) (White et al., 2005).

A possible confusion between leaf folding and snowmelt events is not very likely. On the one hand, every snowy pixel was assumed to be filtered by the algorithm of the ten-day compositing. On the other hand, the comprehensive study of White et al. (2009) showed that the remotely sensed metrics of spring phenology are not correlated generally to the spring snowmelt onset date over the North America forest ecoregions. However, this question remains crucial as the used pre-processing algorithm which filtered both snowy and cloudy pixels was not really designed to detect snow. Future investigations should take advantage of the use of a specific snow detection algorithm designed for forest areas, such as that developed by Delbart et al. (2006) based on SWIR reflectance or of the use of the snow-cover products such as MOD10A1 from MODIS (Simic et al., 2004). *In situ* observations of snow (not available in this study) would also be very useful to investigate possible correlations between the dates of snowmelt and leaf unfolding.

Large unusual disturbances (due to natural environmental factors – e.g. climate, accidents or anthropogenic activities) might have an impact on the annual vegetation dynamics during the five years of the study period. They were rare, except the extreme drought event that occurred in Western Europe in summer 2003. It is possible that the latter had induced in the study area a premature leaf fall during summer and a

disturbance in budburst the following year (Bréda et al., 2006). Moreover, it is likely that averaging data per 100 m wide elevation class attenuated a large part of the possible disturbance effects. Similarly, averaging 5 years of VEGETATION data into a single mean year to fill the large spatio-temporal gaps also contributed to enhance the robustness of characterization of the elevation variations in spring leaf phenology from VEGETATION time-series.

5. Conclusion

This study showed the potential of reflectance time-series at medium resolution, such as those provided by VEGETATION sensors, to monitor the elevation variations in leaf phenology over deciduous broadleaf forests in mountainous regions. The unmixing method of the 1-km² pixels made it possible to analyse the phenological behaviour specific to the deciduous forests when the latter were quite fragmented. The impact of the elevation temperature gradient on the spring leaf phenology was clearly detected over the study area with a high spatial and seasonal consistency of the remote sensing response.

These results were obtained from satellite data averaged over 5 successive years to fill the large spatio-temporal gaps in the VEGETATION time-series due to clouds and snow. Applying a five-year running window over many decades, retrospectively from satellite data time-series accumulated over the most recent 30 years, could provide a robust approach to monitor the trends in long-term changes in the spring leafing timing along elevation gradients as a result of phenology adaptation to climate warming or of changes in the elevation repartition of tree species.

Nevertheless some questions still remain and require more research. In particular, possible effects of snow melting at the time of vegetation growth, and of leaf dynamics and senescence in autumn on the forest remote sensing signatures could not be evaluated in this study. For instance, the processes of leaf loss and colouring in autumn are complex. They may combine the effects of phenology due to elevation variations in temperature and to photoperiod with those due a summer drought. Their interannual variations in comparison with their elevation variations could be larger than for leafing in spring. Therefore, *in situ* continuous measurements of the annual kinetics of snow melting in spring and of green LAI, in addition to the observations of phenology (unavailable in the present study), would be useful in future studies over the study area.

Acknowledgments

This study was partly funded by the PNTS, Programme National de Télédétection Spatiale.

We thank Stephanie Hayes, Heather Lawrence and Ajit Govind for revising the English version of the manuscript. We are grateful for the helpful comments of the anonymous reviewers.

References

- Ahl, D. E., Gower, S. T., Burrows, S. N., Shabanov, N. V., Myneni, R. B., & Knyazikhin, Y. (2006). Monitoring spring canopy phenology of a deciduous broadleaf forest using MODIS. *Remote Sensing of Environment*, 104, 88–95.
- Bacour, C., Bréon, F. M., & Maignan, F. (2006). Normalization of the directional effects in NOAA-AVHRR reflectance measurements for an improved monitoring of vegetation cycles. *Remote Sensing of Environment*, 102, 402–413.
- Badeck, F., Bondeau, A., Böttcher, K., Doktor, D., Lucht, W., Schaber, J., et al. (2004). Responses of spring phenology to climate change. *New Phytologist*, 162, 295–309.
- Baret, F., Hagolle, O., Geiger, B., Bicheron, P., Miras, B., Huc, M., et al. (2007). LAI, fAPAR and fCover CYCLOPES global products derived from VEGETATION: Part 1: Principles of the algorithm. *Remote Sensing of Environment*, 110(3), 275–286.
- Beck, P. S. A., Atzberger, C., Hogda, K. A., Johansen, B., & Skidmore, A. K. (2006). Improved monitoring of vegetation dynamics at very high latitudes: a new method using MODIS NDVI. *Remote Sensing of Environment*, 100, 321–334.
- Beck, P. S. A., Wang, T. J., Skidmore, A. K., & Liu, X. H. (2008). Displaying remotely sensed vegetation dynamics along natural gradients for ecological studies. *International Journal of Remote Sensing*, 29(14), 4277–4283.
- Bertin, R. I. (2008). Plant phenology and distribution in relation to recent climate change. *Journal of the Torrey Botanical Society*, 135, 126–146.
- Bréda, N., Huc, R., Granier, A., & Dreyer, E. (2006). Temperate forest trees and stands under severe drought: a review of ecophysiological responses, adaptation processes and long-term consequences. *Annals of Forest Science*, 63, 625–644.
- Cardot, H., Maisongrande, M., & Faivre, R. (2008). Varying-time random effects models for longitudinal data: unmixing and temporal interpolation of remote sensing data. *Journal of Applied Statistics*, 35(8), 827–846.
- Cleland, E. E., Chuine, I., Menzel, A., Mooney, H. A., & Schwartz, M. D. (2007). Shifting plant phenology in response to global change. *Trends in Ecology & Evolution*, 22(7), 357–365.
- Delbart, N., Le Toan, T., Kergoat, L., & Fedotova, V. (2006). Remote sensing of spring phenology in boreal regions: a free of snow-effect method using NOAA-AVHRR and SPOT-VGT data (1982–2004). *Remote Sensing of Environment*, 101, 52–62.
- EEA (2000). *CORINE land cover technical guide – Addendum 2000, Technical report No 40, May 2000, European Environment Agency, Copenhagen, Denmark 105pp.*
- Fisher, J. I., Mustard, J. F., & Vadeboncoeur, M. A. (2006). Green leaf phenology at Landsat resolution: scaling from the field to the satellite. *Remote Sensing of Environment*, 100, 265–279.
- Fisher, J. I., Richardson, A. D., & Mustard, J. F. (2007). Phenology model from surface meteorology does not capture satellite-based greenup estimations. *Global Change Biology*, 13(3), 707–721.
- Foody, G. M., & Cox, D. P. (1994). Sub-pixel land cover composition estimation using a linear mixture model and fuzzy membership functions. *International Journal of Remote Sensing*, 15, 619–631.
- Gao, F., Morissette, J., Wolfe, R., Ederer, G., Pedelty, J., Masuoka, E., et al. (2008). An algorithm to produce temporally and spatially continuous MODIS-LAI time series. *IEEE Transactions on Geoscience and Remote Sensing*, 5, 60–64.
- Gilbert, M. A., Gonzalez-Piqueras, J., Garcia-Haro, F. J., & Meli, J. (2002). A generalized soil-adjusted vegetation index. *Remote Sensing of Environment*, 82, 303–310.
- Guyon, D., Cardot, H., Hamel, S., & Hagolle, O. (2006). Monitoring and mapping the phenology of the maritime pine forests of South-Western France from VEGETATION time-series. *2nd International Symposium on Recent Advances in Quantitative Remote Sensing (RAQRS'II), Torrent (Valencia) Spain, 25–29 September 2006* (pp. 450–454).
- Hagolle, O., Lobo, A., Maisongrande, P., Cabot, F., Duchemin, B., & De Pereyra, A. (2005). Quality assessment and improvement of temporally composited products of remotely sensed imagery by combination of VEGETATION 1 & 2 images. *Remote Sensing of Environment*, 94, 172–186.
- Hartigan, J. A., & Wong, M. A. (1979). A K-means clustering algorithm. *Applied Statistics*, 28, 100–108.
- Huete, A., Didan, K., Miura, T., Rodriguez, E. P., Gao, X., & Ferreira, L. G. (2002). Overview of the radiometric and biophysical performance of the MODIS vegetation indices. *Remote Sensing of Environment*, 83, 195–213.
- Lenoir, J., Gégout, J. C., Marquet, P. A., de Ruffray, P., & Brisse, H. (2008). A Significant Upward Shift in Plant Species Optimum Elevation During the 20th Century. *Science*, 320, 1768–1771. doi:10.1126/science.1156831 (in Reports).
- Maignan, F., Breon, F. M., Bacour, C., Demarty, J., & Poiron, A. (2008). Interannual vegetation phenology estimates from global AVHRR measurements – Comparison with *in situ* data and applications. *Remote Sensing of Environment*, 112, 496–505.
- Menzel, A., & Fabian, P. (1999). Growing season extended in Europe. *Nature*, 397(6721), 659–659.
- Menzel, A., Sparks, T. H., Estrella, N., Koch, E., Aasa, A., Ahas, R., et al. (2006). European phenological response to climate change matches the warming pattern. *Global Change Biology*, 12, 1969–1976.
- Myneni, R. B., Keeling, C. D., Tucker, C. J., Asrar, G., & Nemani, R. R. (1997). Increased plant growth in the Northern high latitudes from 1981–1991. *Nature*, 386, 698–702.
- Peñuelas, J., & Boada, M. (2003). A global change-induced biome shift in the Montseny mountains (NE Spain). *Global Change Biology*, 9(2), 131–140.
- Rautiainen, M., Nilson, T., & Lukk, T. (2009). Seasonal reflectance trends of hemiboreal birch forests. *Remote Sensing of Environment*, 113, 805–815.
- Richardson, A. J., & Wiegand, C. L. (1977). Distinguishing vegetation from soil background information. *Photogrammetric Engineering and Remote Sensing*, 43, 1541–1552.
- Robin, J., Dubayah, R., Sparrow, E., & Levine, E. (2008). Monitoring start of season in Alaska with GLOBE, AVHRR, and MODIS data. *Journal of Geophysical Research-Biogeosciences*, 113(G1) Article Number: G01017 FEB 26 2007.
- Rondeaux, G., Steven, M., & Baret, F. (1996). Optimization of soil-adjusted vegetation indices. *Remote Sensing of Environment*, 55(2), 95–107.
- Roujean, J. L., Leroy, M., & Deschamps, P. Y. (1992). A bidirectional reflectance model of the Earth's surface for the correction of remote sensing data. *Journal of Geophysical Research*, 97, 20455–20468.
- Rutishauser, T., Luterbacher, J., Jeanneret, F., Pfister, C., & Wanner, H. (2007). A phenology-based reconstruction of inter-annual changes in past spring seasons. *Journal of Geophysical Research*, 2007(112), G04016.
- Simic, Fernandes, R., Brown, R., Romanov, P., & Park, W. (2004). Validation of VEGETATION, MODIS, and GOES + SSM/I snow-cover products over Canada based on surface snow depth observations. *Hydrological Process*, 18, 1089–1104.
- Soudani, K., le Maire, G., Dufrene, E., François, C., Delpierre, N., Ulrich, E., et al. (2008). Evaluation of the onset of green-up in temperate deciduous broadleaf forests derived from Moderate Resolution Imaging Spectroradiometer (MODIS) data. *Remote Sensing of Environment*, 112, 2643–2655.
- Stöckli, R., & Vidale, P. L. (2004). European plant phenology and climate as seen in a 20-year AVHRR land-surface parameter dataset. *International Journal of Remote Sensing*, 25, 3303–3330.
- Thayn, J. B., & Price, K. P. (2008). Julian dates and introduced temporal error in remote sensing vegetation phenology studies. *International Journal of Remote Sensing*, 29(20), 6045–6049.

- USGS (2005). Shuttle Radar Topography Mission, 3 Arc Second scenes, Filled finished-A. *Global Land Cover Facility, University of Maryland, Maryland* (<http://glcf.umd.edu/data/srtm>).
- Vitasse, Y., Delzon, S., Dufrêne, E., Pontailler, J. -Y., Louvet, J. -M., Kremer, A., et al. (2009). Leaf phenology sensitivity to temperature in European trees: do within-species populations exhibit similar responses? *Agricultural and Forest Meteorology*, *149*, 735–744.
- Vitasse, Y., Porté, A. J., Kremer, A., Michalet, R., & Delzon, S. (2009). Responses of canopy duration to temperature changes in four temperate tree species: relative contributions of spring and autumn leaf phenology. *Oecologia*, *161*, 187–198. doi:10.1007/s00442-00961363-4
- White, M. A., De Beurs, K. M., Didan, K., Inouye, D. W., Richardson, A. D., Jensen, O. P., et al. (2009). Intercomparison, interpretation, and assessment of spring phenology in North America estimated from remote sensing for 1982–2006. *Global Change Biology*, *15*, 2335–2359.
- White, M. A., Hoffman, F., Hargrove, W. W., & Nemani, R. R. (2005). A global framework for monitoring phenological responses to climate change. *Geophysical Research Letters*, *32*, L04705. doi:10.1029/2004GL021961
- Zhang, X., Friedl, M., & Schaaf, C. (2009). Sensitivity of vegetation phenology detection to the temporal resolution of satellite data. *International Journal of Remote Sensing*, *30*, 2061–2074.
- Zhang, X., Friedl, M. A., Schaaf, C. B., Strahler, A. H., Hodges, J. C. F., Gao, F., et al. (2003). Monitoring vegetation phenology using MODIS. *Remote Sensing of Environment*, *84*, 471–475.
- Zhou, L., Tucker, C. J., Kaufmann, R. K., Slayback, D., Shabanov, N. V., & Myneni, R. B. (2001). Variations in northern vegetation activity inferred from satellite data of vegetation index during 1981 to 1999. *Journal of Geophysical Research*, *106*, 20 069–20 083.